Master's Thesis of Science

Interannual to Decadal Variability of the Korea Strait Bottom Cold Water during 1982–2021

1982–2021년 기간 대한해협 저층냉수의 장기 변동성

August 2023

School of Earth and Environmental Sciences
Graduate School
Seoul National University

Hyunwoo Lee

Interannual to Decadal Variability of the Korea Strait Bottom Cold Water during 1982–2021

Supervisor: Hanna Na, Professor

Submitting a master's thesis of
Science

May 2023

School of Earth and Environmental Sciences
Graduate School
Seoul National University

Hyunwoo Lee

Confirming the master's thesis written by
Hyunwoo Lee
July 2023

Chair Yang-Ki Cho (Seal)
Vice Chair SungHyun Nam (Seal)
Examiner Hanna Na (Seal)

Abstract

The Korea Strait serves as an inlet of the East Sea since the Tsushima Warm Current, a branch of the Kuroshio Current, flows into it through the Korea Strait. The major water masses in the Korea Strait include the Tsushima Warm Water (with temperatures above 10° C and salinity exceeding 34.3 psu), transported by the Tsushima Warm Current, and the Korea Strait Bottom Cold Water (KSBCW) characterized by temperatures below 10° C, predominantly found at greater depths in the western channel of the Strait. In this study, long-term variations of the KSBCW were analyzed using *in situ* temperature data obtained from the Korea Oceanographic Data Center from 1982 to 2021. The vertical temperature section of the Korea Strait exhibits an interannual variation of the KSBCW as its primary mode of variability on time scales longer than the seasonal cycle. The second most significant mode reflects an enhancement of both the KSBCW and the Tsushima Warm Water since the mid-1990s, implying a strengthening of vertical stratification. The first mode shows a significant relationship with the upper-layer water temperature variability in the southwestern part of the East Sea. The regression analysis using the ERA5 wind fields targeting the first mode reveals that the KSBCW is strengthened, associated with basin-scale counterclockwise wind-stress curl anomalies. The second mode,

however, is suggested to be related to clockwise wind-stress curl anomalies. The relationship between the KSBCW variability and the basin-scale wind variations suggests future works exploring the link with larger-scale climate variations in the broader North Pacific.

Keyword: Korea Strait Bottom Cold Water, East Sea, Interannual variation, Decadal variation, Wind stress

Student Number: 2021-23550

Table of Contents

List of Figures

1. Introduction

1.1. Background

The Korea Strait is a key conduit through which the Kuroshio Current, a major western boundary current in the North Pacific, flows into the East Sea (Isobe, 1994). Within the confines of this strait, a bifurcation occurs based on proximity to Tsushima Island, resulting in two distinct channels: the Western Korea Strait, closer to the Korean Peninsula, and the Eastern Korea Strait, closer to the Japanese coast (Figure 1.1).

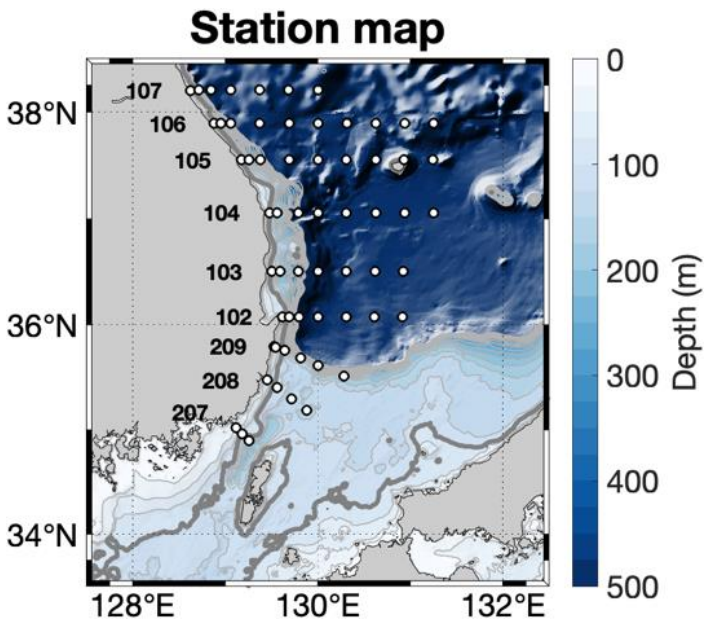

Figure 1.1. Station map with bathymetry. The bold gray line denotes the depth of 100 m.

With its depth and width, the Western Korea Strait, approximated at 200 meters and 42 kilometers, respectively, presents as a comparatively deeper and narrower waterway. In contrast, the Eastern Korea Strait, with a depth of around 140 meters and extending approximately 100 kilometers in width, is discernibly shallower and broader (Cho & Kim, 2000).

In the Western Korea Strait, two primary water masses can be observed. The first is characterized by temperatures exceeding 10° C and salinity levels greater than 34.3 psu, corresponding to the traits of the Tsushima Warm Water (Kim & Kim, 1983; Lim & Chang, 1969; Teague et al., 2006). The second water mass, the Korea Strait Bottom Cold Water (KSBCW), exhibits temperatures below 10° C (Figure 1.2). Some previous studies have discussed the importance of understanding the KSBCW to gain insights into the characteristics of the southwestern East Sea (Kim, Cho, & Kim, 2018).

The KSBCW is known to exhibit pronounced variations over time (Chang et al., 2004; Cho & Kim, 1998; Isobe, 1995; Johnson & Teague, 2002; Kim et al., 2006; Min, Kim, & Kim, 2006; Min et al., 2011; Na et al., 2009; Na et al., 2010). The figure under discussion is drawn from the work published by Min et al. (2011). The authors conducted quasi-monthly temperature observations from March 2006 to November 2010 at the indicated point using Conductivity, Temperature, and Depth (CTD) measurements. Their findings indicated that, during the observation period, the KSBCW was detected at the observation point during August, September, and October of 2006; September and

October of 2007; and July, August, and September of 2010. In contrast, cold water with temperatures below 10 degrees Celsius was not observed at the location in 2008 and 2009. These results highlight the intermittent nature of the KSBCW presence, evidencing irregular fluctuations in its strength.

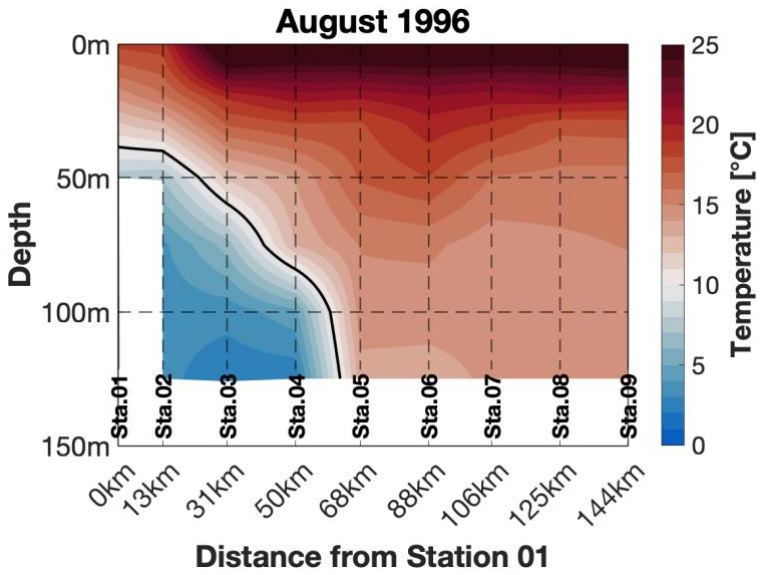

Figure 1.2. Vertical temperature section of the KODC line 208 in August, 1996. The black solid line denotes the 10°C contour.

The KSBCW is reportedly associated with a southward current observed at the depths of the western channel of the Korea Strait (Nam et al., 2016; Park, 2016; Park, Cho, & Kim, 1995; Perkins et al., 2000; Teague et al., 2006). As can be seen from the velocity measurements performed at the indicated point from June to October 1999, there was a persistent southward current at depths greater than 170 meters

throughout the observation period. Several studies suggested that the KSBCW is the manifestation of a cold water mass originating within the East Sea, which is then transported into the Korea Strait by this southward current (Kim & Lee, 2004; Kim et al., 2006; Yoon & Kim, 2009). This perspective draws a direct correlation between the southward current and the detection of KSBCW within the region.

Yoon et al. (2004) exhibited a connection between the KSBCW and the North Korean Cold Water (NKCW). From April to August 1996, cold water expansion headed south along the East Sea coastline. Conversely, the influence of the cold water appears to diminish from October to February (Yun et al., 2004). The cold water stream that originates from the northern coast of the East Sea and moves southward is referred to as the North Korean Cold Current (NKCC). The NKCC transports the NKCW, observable near Line 107 in Sokcho in April, and arrives south of the Ulleung Basin roughly one to two months later.

Yoon et al. (2004) proposed that a sill between the Ulleung Basin and the Korea Strait prevents the NKCW from flowing directly into the Strait. Instead, the NKCW accumulates for two to three months before it surpasses the sill and enters the Korea Strait. Therefore, this research indicates that the NKCW observed near Sokcho in April can become the source of the KSBCW observed in the Korea Strait in August and September.

The East Sea Intermediate Water (ESIW), originating from the northern East Sea (Kim & Kim, 1999), is the origin of the NKCW. In a

comprehensive study by Nam et al., 2016, significant decadal oscillations in the physical properties of ESIW, traced along isopycnal layers, were observed and linked to the Arctic Oscillation (AO). During periods of positive AO, intensified cold-air outbreaks increase the density of the ESIW, indicating a crucial connection between atmospheric and oceanic phenomena (Nam et al., 2016).

Simultaneously, the intensity of the KSBCW intrusion is affected by tidal forces, particularly energetic semidiurnal internal tides. Furthermore, variations in the circulation patterns, such as those in the East Korea Warm Current (EKWC), can significantly impact the characteristics of ESIW and, potentially, the KSBCW intrusion. For instance, in 2010, ESIW was observed to be colder and fresher than in 2001, a change attributed to a less pronounced EKWC.

The combined influence of the AO, tidal forces, and EKWC on the ESIW and KSBCW reveals the complex interplay of climatic and oceanic dynamics in this region, necessitating further investigation to unravel their interconnected influences.

The mechanism for its intensified intrusion during summer remains unclear. Park et al. (2016) use numerical simulations with a high-resolution regional ocean model to explore if tides can influence the strength of KSBCW intrusion (Park et al., 2016). The model covers the Korea Strait and the southwestern East Sea, with simulations conducted for various cases, incorporating semidiurnal tides (M2 S2), diurnal tides (K1 O1), and different wind forcings. The results reveal that energetic semidiurnal internal tides, generated around the

continental shelf in the northern part of the Korea Strait, can stimulate KSBCW intrusion via the internal tidal pumping effect.

Simulations that included the four major tides best reproduced a dome-shaped bottom cold water mass (below 10° C) impacting the southeast coast of Korea's slope. That is in line with historical monthly mean temperature fields. Supporting the simulation results, long-term (>10 years) ferry boat ADCP measurements across the Korea Strait show that southwestward KSBCW intrusions strengthen 2-3 days after spring tides in summer and fall when the semidiurnal internal tides are heightened. They propose that the energetic semidiurnal internal tides induce the maximum KSBCW intrusion observed in August/September.

In Na et al. (2010), the importance of wind as a factor inducing interannual variations in the KSBCW was derived from their work. This study examined the interannual variations of KSBCW over 35 years, from 1962 to 1996. Utilizing statistical methods to identify wind fields associated with these temporal variations, they found that winds blowing southward along the East Sea coast were prevalent, exhibiting a counterclockwise rotating component. They demonstrate a high correlation between the calculated temporal variations from the correlation of such wind fields with KSBCW and the interannual variations of the KSBCW. These findings revealed that variations in the East Sea basin-scale wind field could account for the interannual variations observed in the KSBCW. There are other studies on the variations of wind effect on the East Sea, which can induce the variability of KSBCW (Gordon & Giulivi, 2004; He et al., 2017; Lyu &

Kim, 2002; Na et al., 2018; Pak et al., 2014; Park, 2018; Park, Park, & Kang, 2022; Yeo, Kim, & Kim, 2017; Yoon et al., 2005; Yoon et al., 2016).

1.2. Objectives

This research aims to deepen our understanding of the interannual to decadal variability of the KSBCW and its dynamic interactions with wind and oceanic parameters. First, probe the interannual variability of the KSBCW in an expanded temporal frame from 1980 to 2021. This contemporary assessment aims to provide updated insights, building upon and extending the work of Na et al. (2010), which examined this variability from 1962 to 1996. Second, explore the linkages between the KSBCW and the upper-ocean temperature variability in the southwestern East Sea. The goal is to investigate the role of these temperature variations in influencing the behavior and properties of the KSBCW. Last, investigate the association between the KSBCW and wind variability related to the Arctic Oscillation. This examination aims to shed light on how much broad-scale atmospheric patterns can shape the characteristics of the KSBCW. Through these points, the research strives to deepen the scientific discourse around the complexities of the KSBCW and its relationship with broader oceanographic and atmospheric phenomena.

2. Data and Methods

2.1. Data

This study uses two primary sources of data: the upper water temperature data, sourced from the Korea Oceanographic Data Center (KODC), and the surface wind data, obtained from the European Centre for Medium-Range Weather Forecasts (ECMWF) Reanalysis v5 (ERA5) which is produced by the Copernicus Climate Change Service (C3S) at ECMWF. The data period used is from 1979 to 2022.

The temperature data are obtained on mostly bimonthly cruise surveys conducted by the National Institute of Fisheries Science from February to December. The stations used in this study are in the East Sea (Line 208 - Line 102) and Line 207. Some station data were obtained until 1998, so that station data is ignored. The temperature data are provided at 14 vertical levels (0, 10, 20, 30, 50, 75, 100, 125, 150, 200, 250, 300, 400, and 500 m).

Temperature data were predominantly collected in the even months (Lee et al., 2010). However, there are exceptions due to specific climatic conditions that occasionally prevented data collection during these months. At a depth of 100m at Station 2, along line 208, for instance, these exceptions occurred in September 1992; September and November 1999; January and March 2000; May 2004; May, September, and November 2006; March 2009; March and September 2010; September 2011 and 2012; November 2015; March

2018; July 2019; and November 2020 and 2021. The monthly temporal interpolation was applied to modify the impact of this uneven distribution.

2.2. Methods

The temperature data under investigation ranged from a minimum of 0.01 degrees Celsius to a maximum of 31.0565 degrees Celsius during the study period. An interpolation method that preserves the original data range was necessary, given the data constraints. The spline method resulted in a minimum interpolated temperature of −1.8 degrees Celsius, indicating that this method made unrealistic negative temperatures. Similarly, the Modified Akima Piecewise Cubic Hermite interpolation method produced a minimum value of −0.30 degrees Celsius. In contrast, the Piecewise Cubic Hermite interpolating Polynomial (pchip) method maintained the realistic temperature range, with the minimum interpolated temperature aligning with the original minimum of 0.01 degrees Celsius. Therefore, this study chose the pchip method for interpolating temperature values. For handling depth variation, 1-m linear interpolation was applied. The temperature and wind data anomaly were carried out to eliminate seasonal biases by subtracting monthly climatology from each dataset. A 13-month low pass filter was applied to both temperature and wind anomalies to eliminate annual variation further.

In choosing the appropriate location for our study of long-term variations of the KSBCW, a comparative analysis of the deepest

standard depths at station 03 of lines 207, Station 02, Station 03, and station 04 of line 208 was conducted (Figure 2.1). The data revealed that Station 2 at line 208, at a depth of 100m, consistently showed the coldest mean temperature around 10 degrees Celsius. This distinction showed line 208 as a critical area for observing KSBCW variations. Further examination of the climatology of line 208 established August as the season with the coldest temperatures (Figure 2.2).

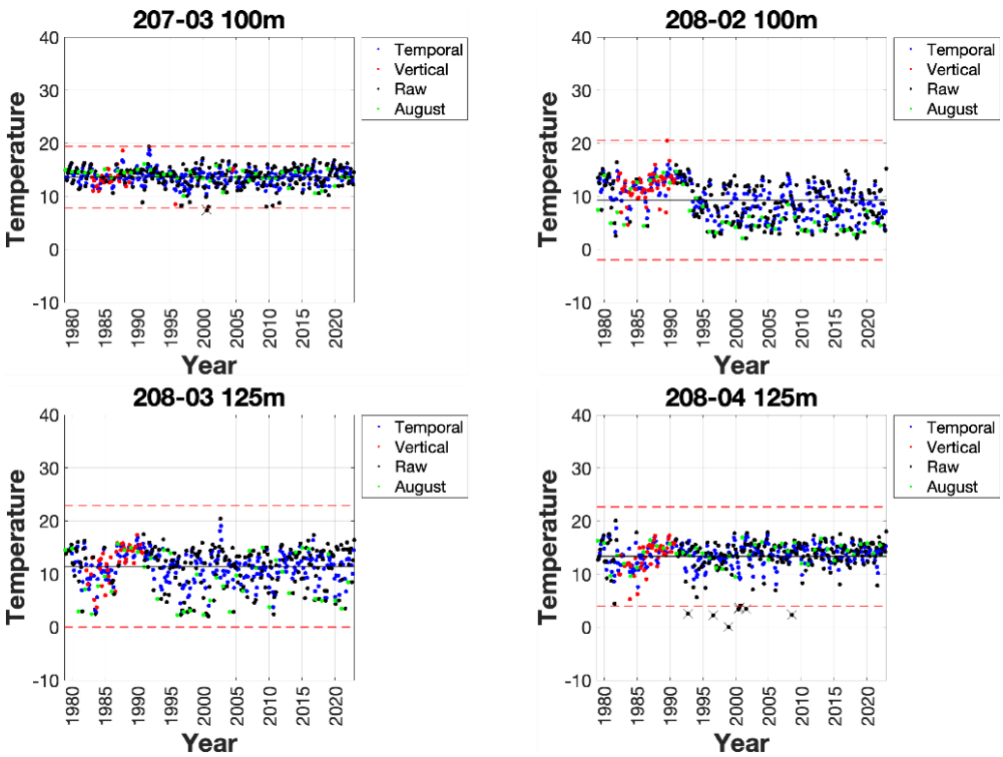

Figure 2.1. Comparison of the temperature at the deepest depth of station 03 in line 207 (top left), and stations 02 (top right), 03 (bottom left), and 04 (bottom right) in line 208.

Following data preprocessing, to investigate KSBCW variability, an Empirical Orthogonal Function (EOF) analysis was performed on the temperature data at the line 208 station. The EOF analysis helped to capture significant variability patterns within the data. However, the EOF analysis of the data indicated a degree of consistency compared to low-pass filtered anomalies. Despite the seasonal variation seen in the raw climatological data, the patterns of variation in the filtered anomalies did not show drastic differences. That provided additional support for selecting line 208 as the focus of this study, demonstrating its suitability for capturing the essential characteristics of KSBCW variations.

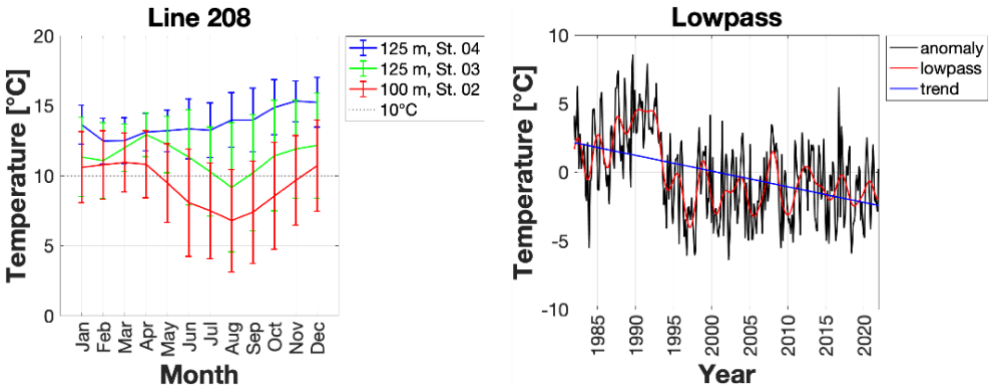

Figure 2.2. The seasonal climatology of the temperature (left) and temperature anomalies (right) at the bottom depth of the Korea Strait.

Surface Turbulent Heat Flux (THF) denotes the summation of the surface sensible heat flux and the surface latent heat flux. This

composite heat flux represents the energy exchange through both convective and evaporative processes at the air-sea interface, influencing many oceanic dynamics, from surface temperature variability to deep ocean circulation.

3. Results

3.1. Climatology

Examining the spatial temperature distributions in the southwestern East Sea reveals colder temperatures closer to the shore and at greater depths (Figure 3.1). This pattern is particularly pronounced in regions where temperatures drop below 10 degrees Celsius, typically observed at a depth of 100m in the Korea Strait.

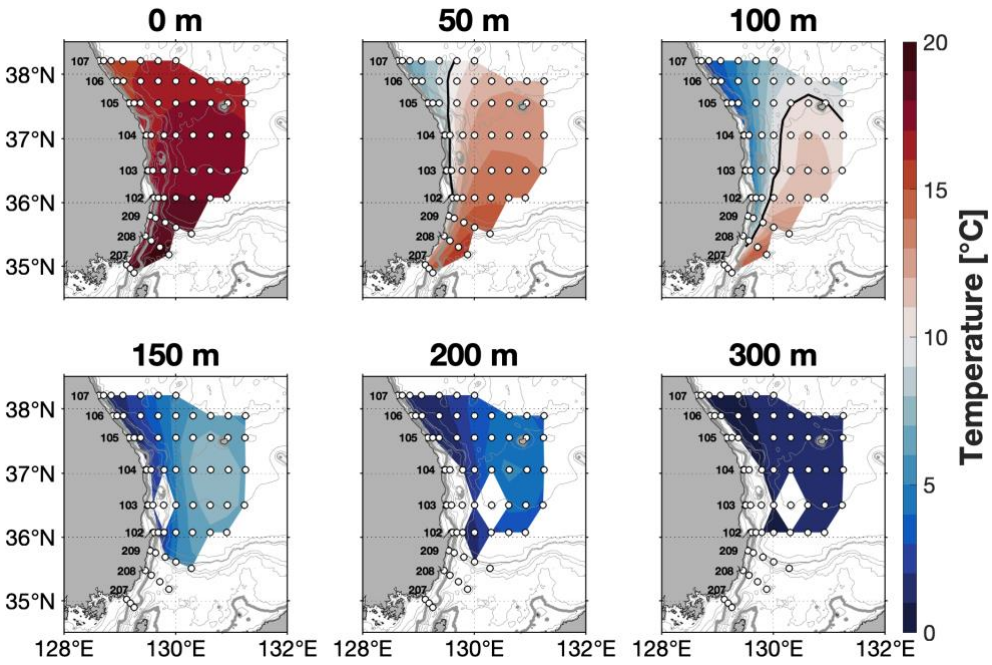

Figure 3.1. The horizontal distribution of the mean temperature. The black line denotes the 10°C contour.

Further analysis of the vertical temperature sections along each line reinforces these findings (Figure 3.2). Consistently, temperatures

registered below 10°C at a depth of 100m in Line 208. This consistency underscores the influence of depth and proximity to the shore on the temperature profile of the water mass. These characteristics further substantiate the selection of Line 208 and the 100m depth level for the detailed study of the long-term variations of the KSBCW.

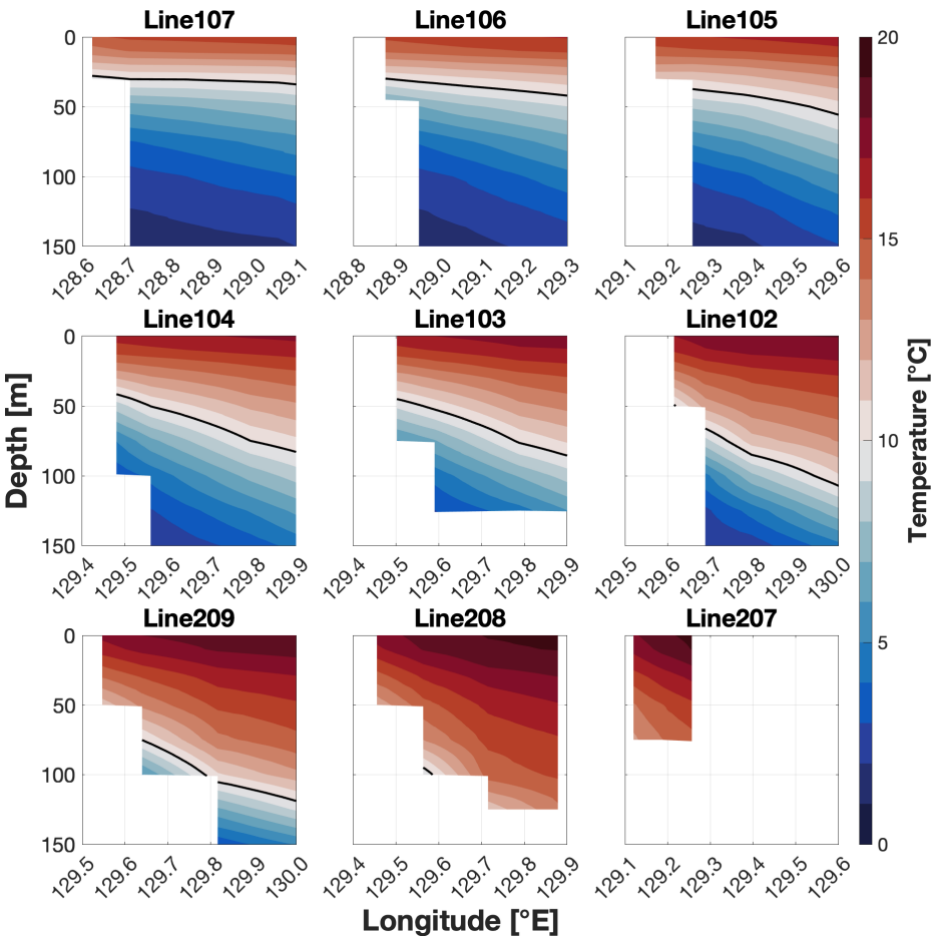

Figure 3.2. The vertical sections of the mean temperature. The black line denotes the 10°C contour.

3.2. KSBCW in Summer

Upon comparing the results of EOF analysis of depth-dependent climate values, derived from both 13-month low-pass filtered monthly anomaly temperature data and summer-specific temperature data (July, August, and September), certain similarities and differences were observed. While the explanatory power of the modes changed, the order of the modes, their spatial distribution, and the PC timeseries remained consistent (Figure 3.3). Furthermore, the spatial distribution of climate values was similarly represented (Figure 3.4). All subsequent results are based on the 13-month low-pass filtered monthly anomaly temperature data.

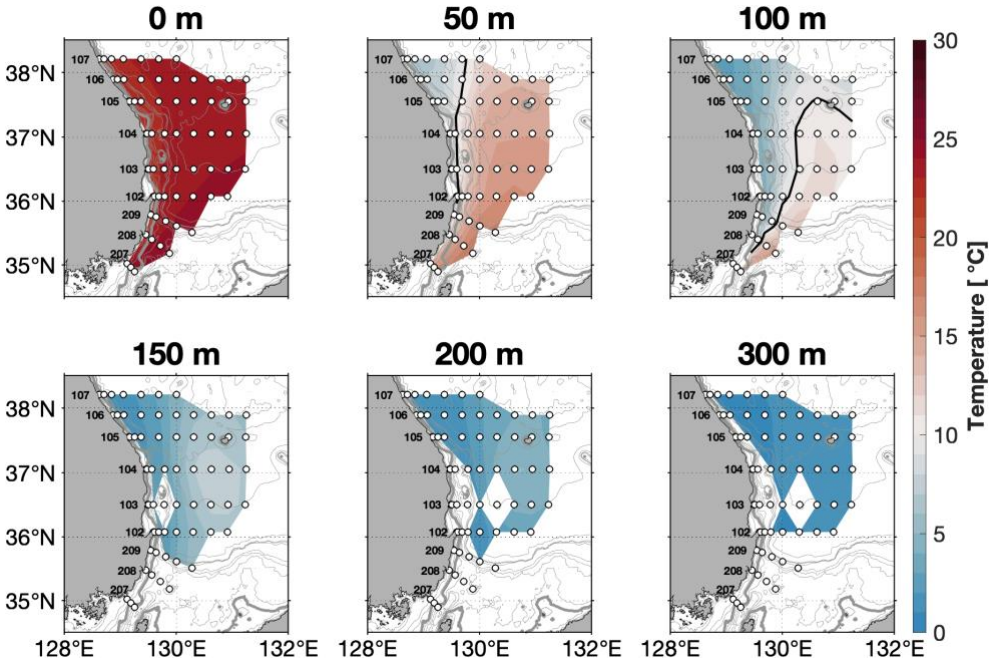

Figure 3.3. The horizontal distribution of the mean temperature in summer. The black line denotes the 10°C contour.

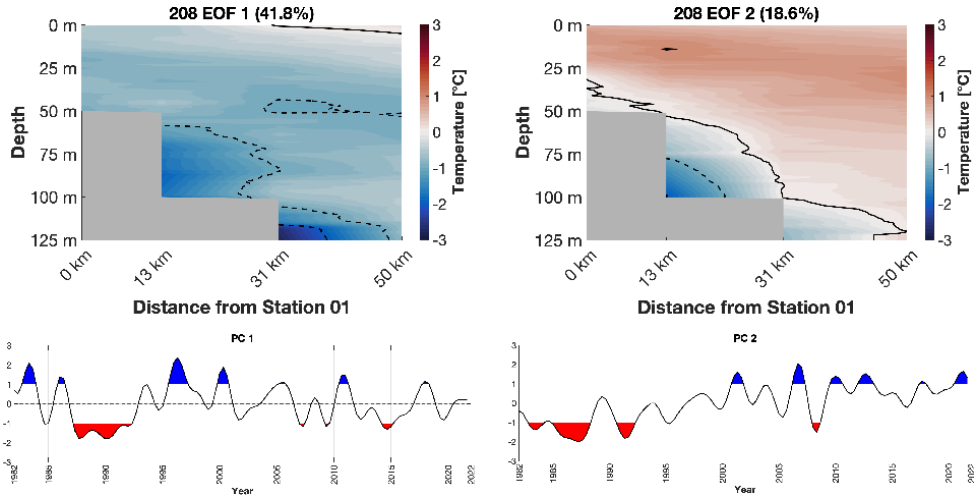

Figure 3.4. The first (left) and second (right) EOF modes of the temperature in line 208 for summer.

3.3. First EOF mode

The first mode accounts for 49.4% of the variance (Figure 3.5). The spatial vector of the first mode exhibits a uniform direction of variability, with the most substantial variability discernible in the lower layers. The Principal Component (PC) timeseries demonstrate interannual variability, leading us to consider this mode as an indicator of the interannual variability of the KSBCW.

In the PC timeseries, periods where the amplitude of variability exceeds +1 are defined as times of KSBCW intensification, while periods, where the amplitude falls below −1 are viewed as times of KSBCW weakening. A composite analysis was conducted based on

these definitions. The spatial variability and the PC timeseries echo the KSBCW fluctuations of the KSBCW reported by Na et al. (Na et al., 2010).

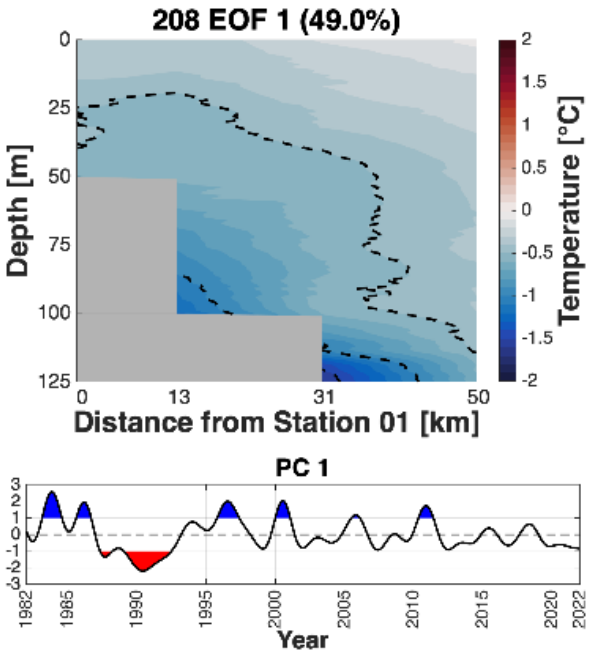

Figure 3.5. The first EOF mode of the temperature in line 208.

Figure 3.6. compares the composite of anomalies during positive and negative periods. During positive periods, there is a discernible intensification of cold water influence. Furthermore, the surface variability is minimal, while the variability is more pronounced in the lower layers. Figure 3.7. depicts the variations in isotherms when the average is added to the anomalies. The distribution of isotherms suggests a contraction of the cold water influence during negative periods and strengthening during positive periods.

Figure 3.8 shows the northernmost longitude (Line 107), south of the Ulleung Basin (Line 209), and Line 208, respectively. These lines were chosen to see the variability of the KSBCW in the vertical cross-section of the anomalies. During the unfavorable period, where the strength of the bottom cold water is weaker, relatively strong warm anomalies appear around the 100m and 150m depth at Lines 209 and 208. Conversely, during the favorable period, where the bottom cold water is strengthened, the temperature at Lines 209 and 208 reveals cold anomalies. Figure 3.9 combines the previous image of anomalies with the average. During negative periods, the isotherms deepen, while they become shallower during positive periods.

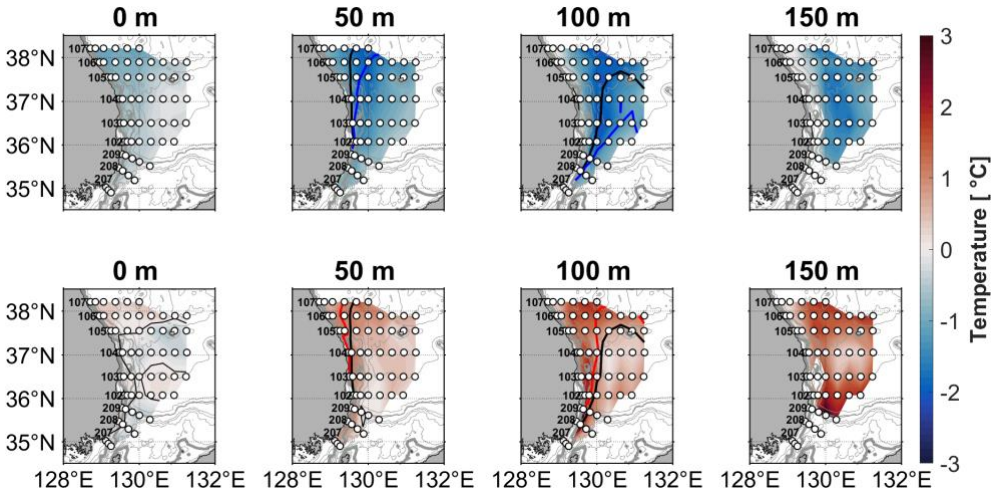

Figure 3.6. Composites of the temperature anomalies based on the EOF mode 1. Black, blue and red lines denote 10°C contour during the entire period, during the positive (PC > + 1) and negative (PC < −1) phases, respectively.

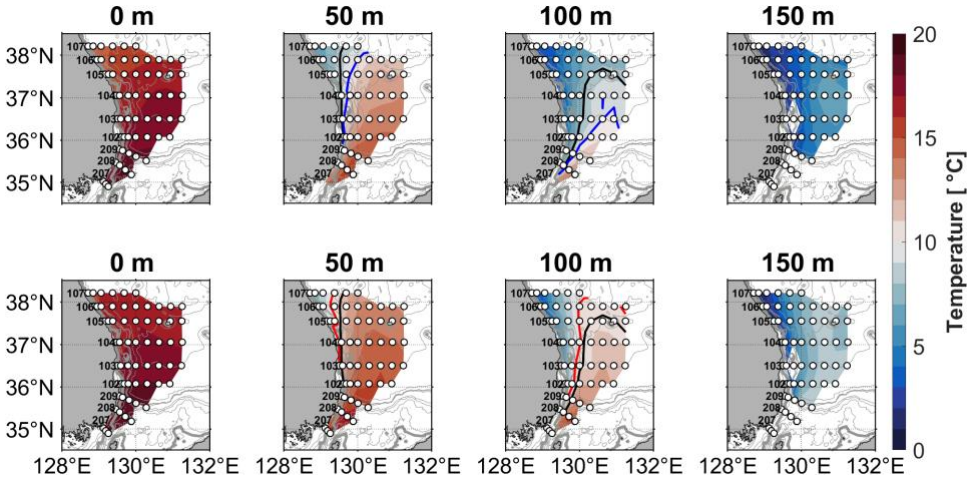

Figure 3.7. Composites of the temperature based on the EOF mode 1. Black, blue and red lines denote 10°C contour during the entire period, during the positive (PC > + 1) and negative (PC < −1) phases, respectively.

The first mode of EOF analysis aligns with findings from Nam et al. (2016) regarding the ESIW. ESIW is formed in the northern East Sea, and its physical properties are determined by wintertime air-sea interaction. Significant decadal oscillations in spiciness were observed, linked to the AO and consequent cold-air outbreaks. During positive AO phases, intermediate water reaches a higher density. That is similar to our EOF analysis, where fluctuations in the intermediate layer temperature could be attributed to similar mechanisms. Furthermore, the distinct characteristics of intermediate water in 2001 and 2010, as investigated by Nam et al., could be captured in our EOF mode, emphasizing the role of the EKWC in modulating these characteristics (Nam et al., 2016).

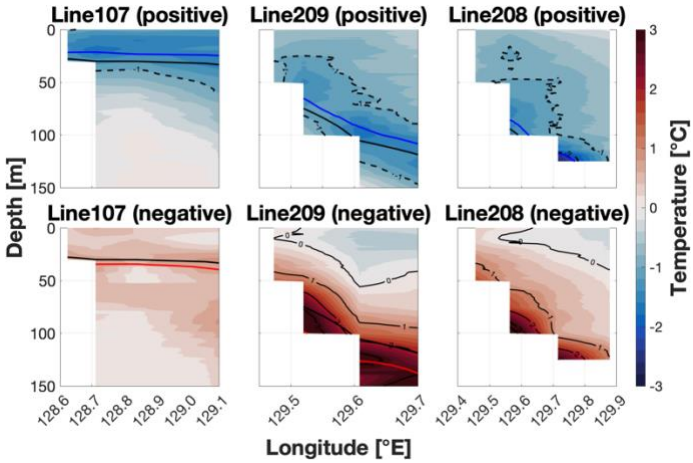

Figure 3.8. The vertical sections of the composites of the temperature anomalies based on the EOF mode 1. Black, blue and red lines denote 10°C contour during the entire period, during the positive (PC > + 1) and negative (PC < −1) phases, respectively.

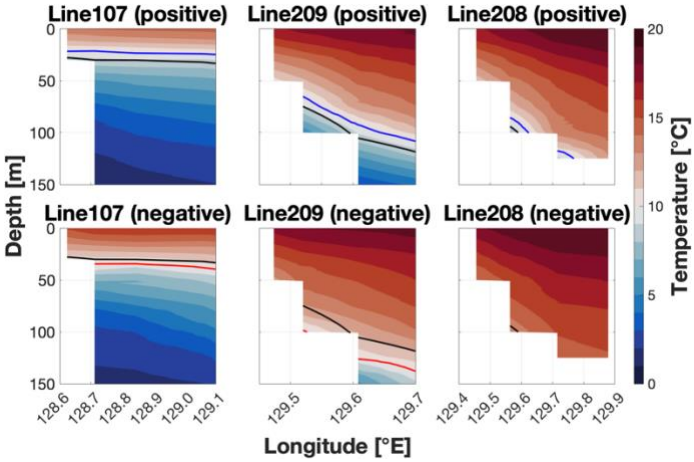

Figure 3.9. The vertical sections of the composites of the temperature based on the EOF mode 1. Black, blue and red lines denote 10°C contour during the entire period, during the positive (PC > + 1) and negative (PC < − 1) phases, respectively.

3.4. Second EOF mode

The second mode of EOF analysis accounts for 30.0% of the total variance (Figure 3.10). Substantial variability is apparent in the coastal bottom layer, whereas relatively weak variability is observed in the offshore surface layer, and these two variabilities exhibit opposite signs. The second mode’s PC timeseries shows a difference around the mid-1990s. Negative anomalies existed from the 1980s until the mid-1990s, after which positive anomalies became prevalent. This pattern suggests a phase shift in the mid-1990s, with the KSBCW becoming much colder and the Tsushima Warm Current becoming much warmer.

Comparing the composite results of the first and second modes (Figure 3.11), unlike the first mode (Figure 3.6), the composite results of the anomalies of the second mode show warm anomalies in the surface layer during the favorable period, warm anomalies in the offshore area at a depth of 100m, and cold anomalies on the coastal side. During the unfavorable period, the opposite is observed. Considering the spatial distribution and PC timeseries of the second mode, after the mid-1990s, it is assumed that the temperature at a depth of 100m on the East Sea coast became lower, while the temperature at shallower depths and in the open sea became higher compared to the previous period.

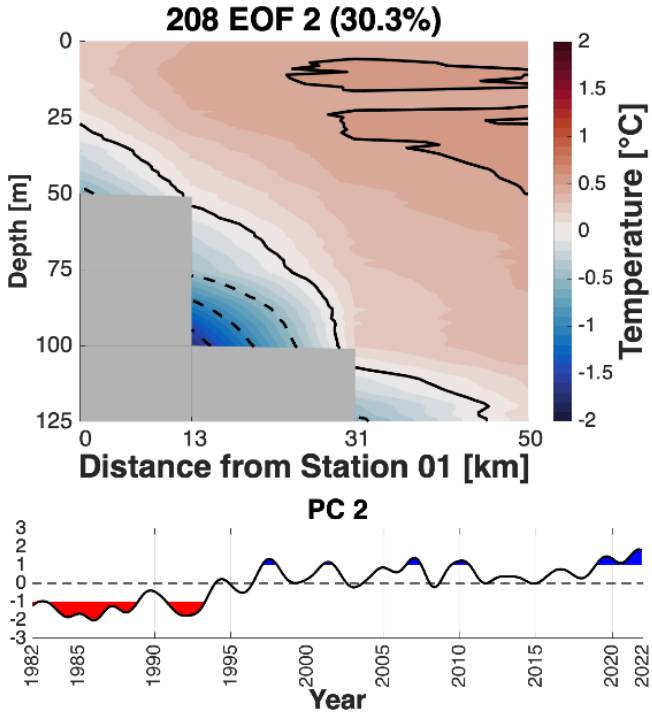

Figure 3.10. The second EOF mode of the temperature in line 208.

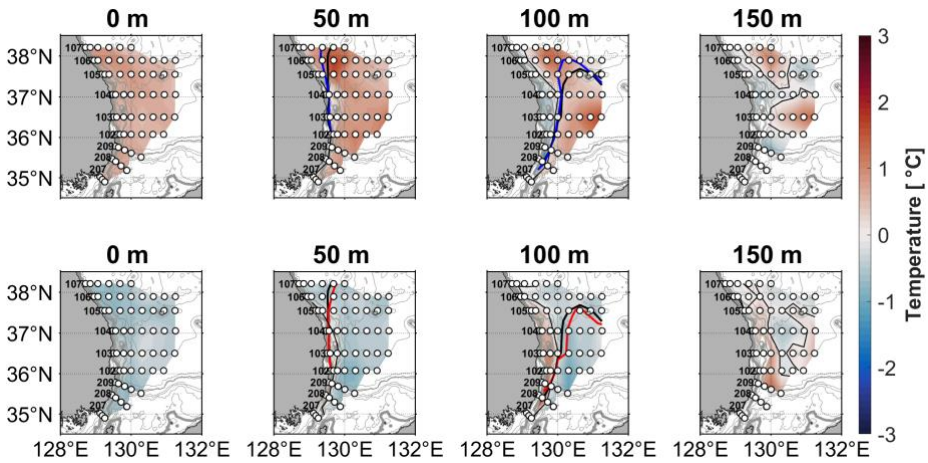

Figure 3.11. Composites of the temperature anomalies based on the EOF mode 2. Black, blue and red lines denote 10°C contour during the entire period, during the positive (PC > + 1) and negative (PC < −1) phases,

respectively.

Figure 3.12 shows the temperature distribution and isotherms after adding the average. Unlike the first mode (Figure 3.3.3), the second mode does not show a significant change in the position of the isotherms. That suggests that the variability of the second mode is related to an increase in the temperature difference between the upper and lower layers.

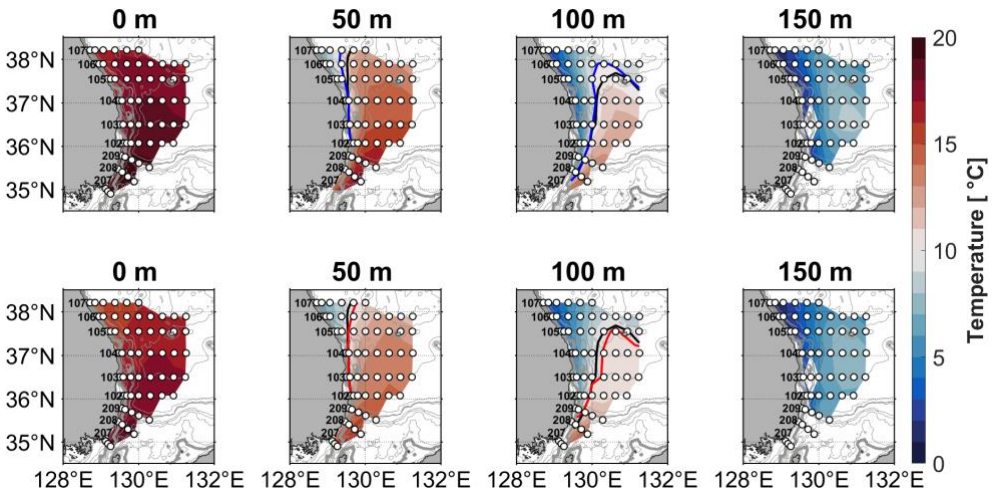

Figure 3.12. The horizontal distribution of the temperature composites based on the EOF mode 2. Black, blue and red lines denote 10°C contour during the entire period, during the positive (PC > + 1) and negative (PC < − 1) phases, respectively.

Figure 3.13 provides the vertical distribution of the temperature anomalies. Unlike the first mode, the second mode shows different

temperature variations between the coastal bottom and surface layers. Compared to the spatial distribution of the first mode (Figure 3.9), which shows more significant variability at greater depths, the second mode shows strong anomalies at relatively shallow depths on the coastal side. When the average is added to the anomalies, the depth of the isotherms shows relatively less variation compared to the first mode (Figure 3.14).

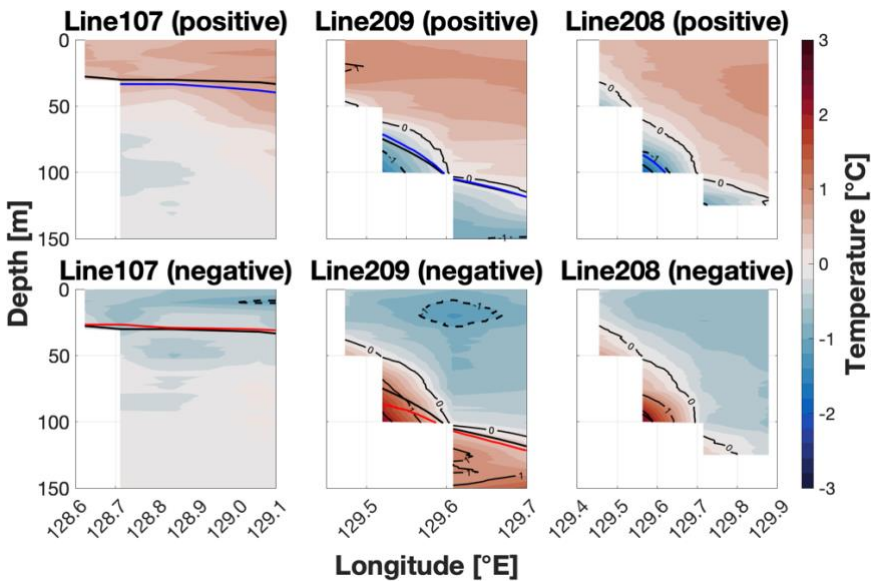

Figure 3.13. The vertical section of the composites of the temperature anomalies based on the EOF mode 2. Black, blue and red lines denote 10°C contour during the entire period, during the positive (PC > + 1) and negative (PC < −1) phases, respectively.

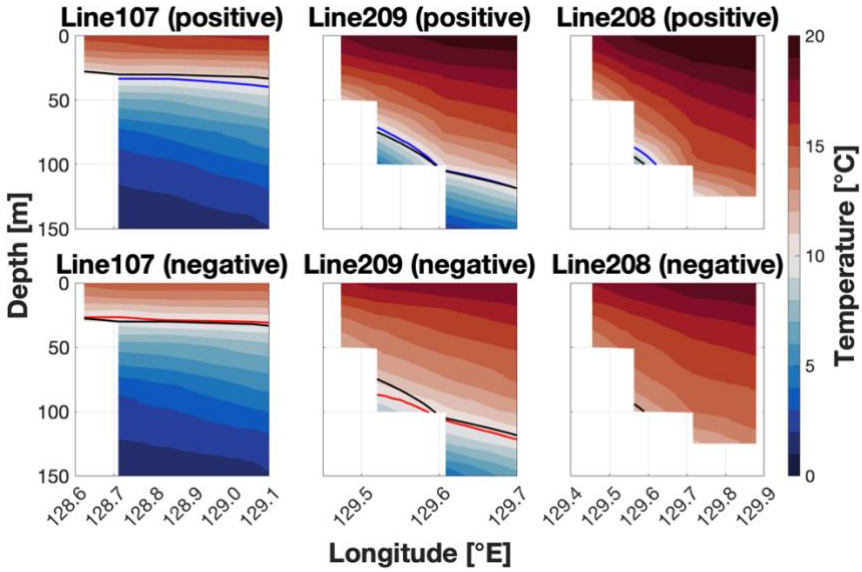

Figure 3.14. Vertical section of the temperature composites based on the EOF mode 2. Black, blue and red lines denote 10°C contour during the entire period, during the positive (PC > + 1) and negative (PC < −1) phases, respectively.

The second EOF mode may provide additional context to the work of Chen et al. (2022) regarding the Subpolar Front (SPF) in the East Sea (Chen et al., 2022). Chen et al. discussed the variability in the intensity and position of the SPF on a decadal timescale and attributed this variability to geostrophic advection, specifically its zonal component. This explanation echoes the patterns revealed in our second EOF mode, which exhibits temperature variations that might be attributed to the same dynamics. Moreover, Chen et al.'s findings on the varying meridional movements of the SPF in the eastern, central, and western regions, alongside their link to the Subpolar Front Current (SFC), offer a possible interpretation for the spatial patterns found in

our EOF mode. Therefore, our study not only corroborates their findings but also expands upon them by identifying similar temperature variability dynamics within the intermediate layers of the ocean.

3.5. Relationship with wind variability

This section describes the results of regression analysis of wind variations on the PC timeseries for each mode. When the first mode intensifies, wind stress anomalies display a counterclockwise rotational component predominant at the scale of the East Sea basin, and the correlation coefficient between the timeseries projected through the regressed wind and the PC timeseries of the first mode is 0.54. Although this coefficient is smaller than prior studies, it suggests a correlation between wind field variability and KSBCW variability (Figure 3.15). When examining wind stress, the positive composite of mode 1 demonstrated a pattern closely aligned with the wind stress regression observed in mode 1 (Figure 3.17. (a), (b)). The negative composite, however, presented an opposing pattern, signifying an inverse relationship (Figure 3.17. (c), (d)).

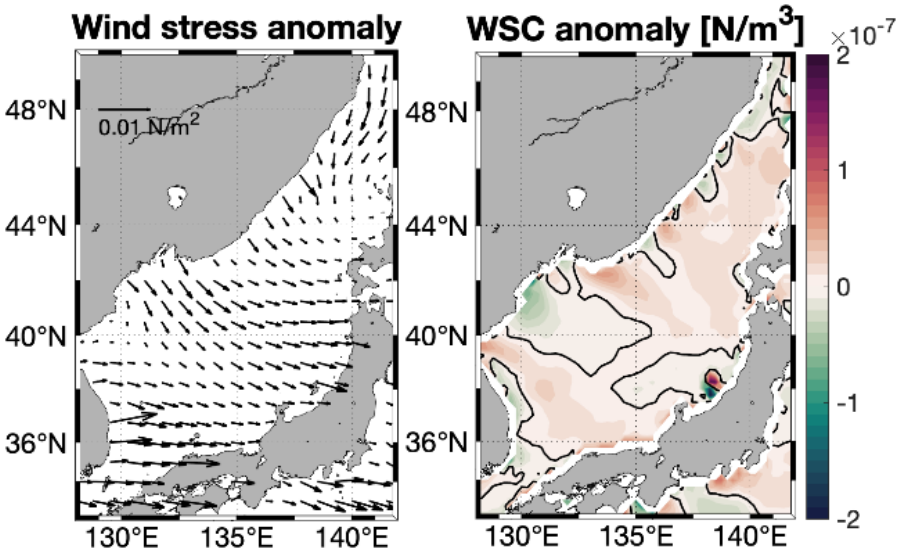

Figure 3.15. Wind stress anomaly regressed on the PC time series of the EOF mode 1.

Unlike the first mode, the wind anomaly field regressed on the second mode manifests as a clockwise rotational component. The correlation coefficient between the projected timeseries and the timeseries variability of the second mode is 0.53, indicating that the variability of the second mode is also correlated with the wind field (Figure 3.16). For mode 2, the positive composite bore a resemblance to the regression pattern, implying a consistent relationship (Figure 3.18 (a), (b)). However, the negative composite for mode 2 did not align as anticipated with the opposite of the regression pattern. This inconsistency indicates potential complex mechanisms at play in the second mode, warranting further investigation (Figure 3.18 (c), (d)).

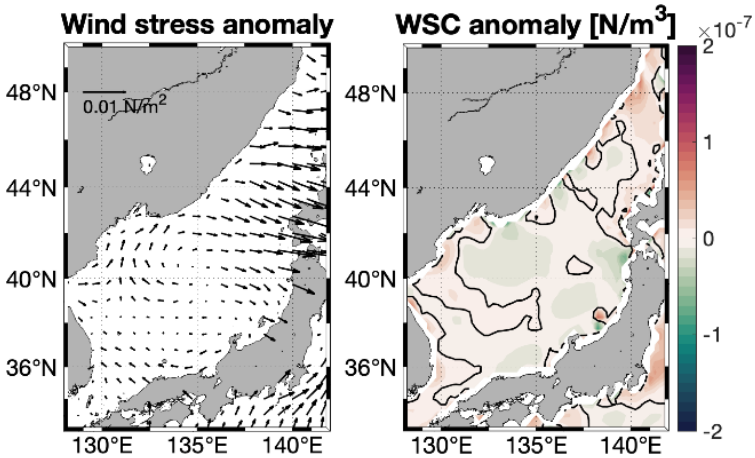

Figure 3.16. Wind stress anomaly regressed on the PC time series of the EOF mode 2.

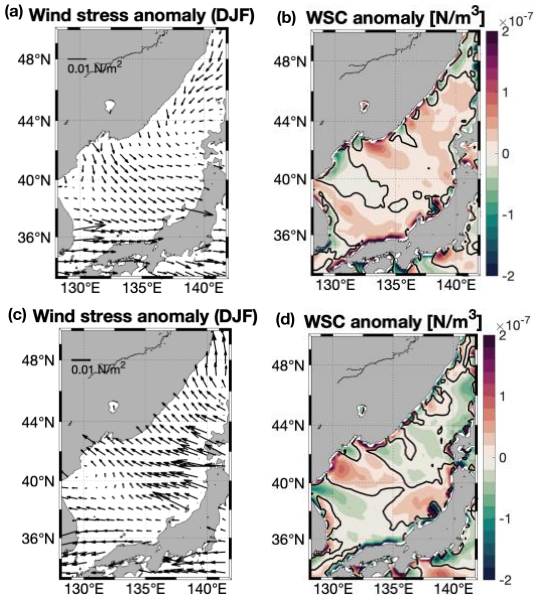

Figure 3.17. Positive (top) and negative (bottom) composites based on the EOF mode 1: (a) wind-stress anomaly, (b) wind-stress curl anomaly, (c) wind-stress anomaly, (d) wind-stress curl anomaly.

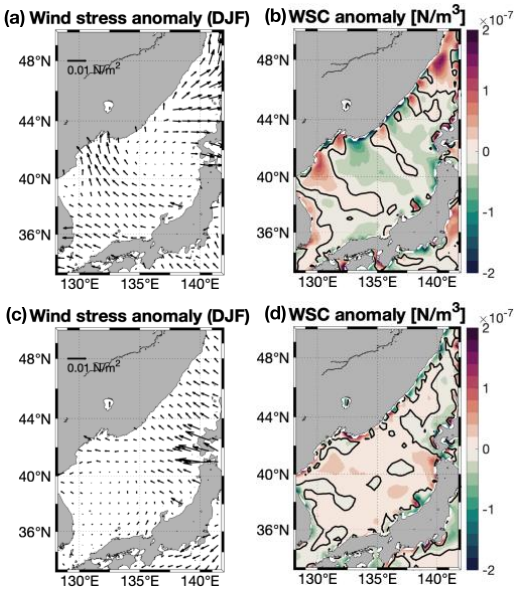

Figure 3.18. Same as Figure 3.17, but for the EOF mode 2.

4. Discussion and Conclusion

An analysis of winter mean Sea Surface Temperature (SST) and 2-meter air temperature differences primarily shows SST values warmer than the T2m, with the exception around the Tsugaru Strait (Figure 4.1). The consistency between the two variables is confirmed by the relatively small standard deviation. Moreover, the mean turbulent heat flux is seen to be directed downward, indicating that the ocean is predominantly absorbing heat during the winter period (Figure 4.2). Areas exhibiting the most significant variability in the turbulent heat flux, as reflected by a larger standard deviation, include southern Vladivostok, western Japan, and the eastern coast of the Korean Peninsula. This suggests that these areas may experience more complex air-sea interactions, affecting the regional heat flux dynamics.

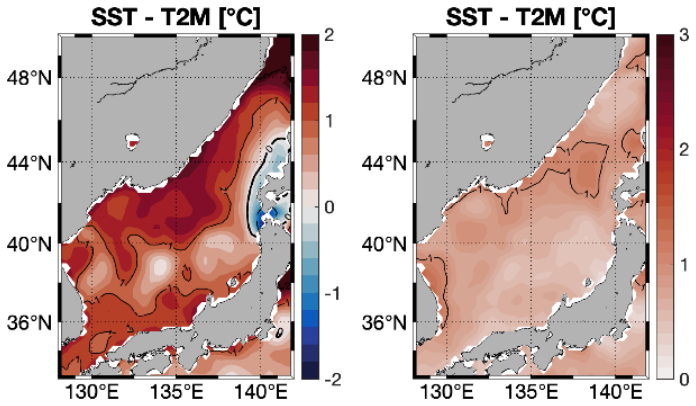

Figure 4.1. Mean (left) and standard deviation (right) of the difference between SST and 2-m temperature in December, January, and February.

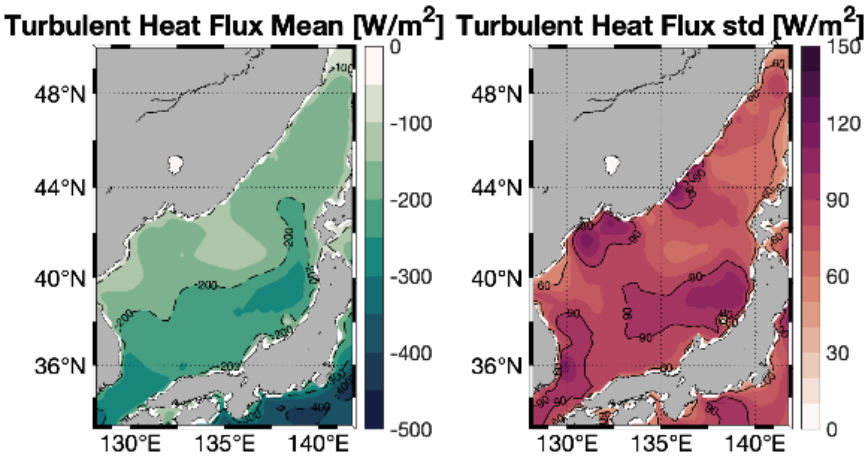

Figure 4.2. Mean (left) and standard deviation (right) of turbulent heat flux in December, January, and February.

Figure 4.3 presents the results of regression analysis of the turbulent heat flux anomalies in the East Sea basin on each mode of the KSBCW. Positive values represent the heat flux flow from the atmosphere to the ocean. Although not shown here, statistically, the turbulent heat flux regressed on the first mode was insignificant. In contrast, the turbulent heat flux regressed on the second mode was significant at the location of the subpolar front. Considering that the second mode is associated with the intensification of the KSBCW and Tsushima Warm Water, it could be hypothesized that the strengthening of the Tsushima Warm Water influences the subpolar front, which may be associated with the turbulent heat flux. These require further analysis.

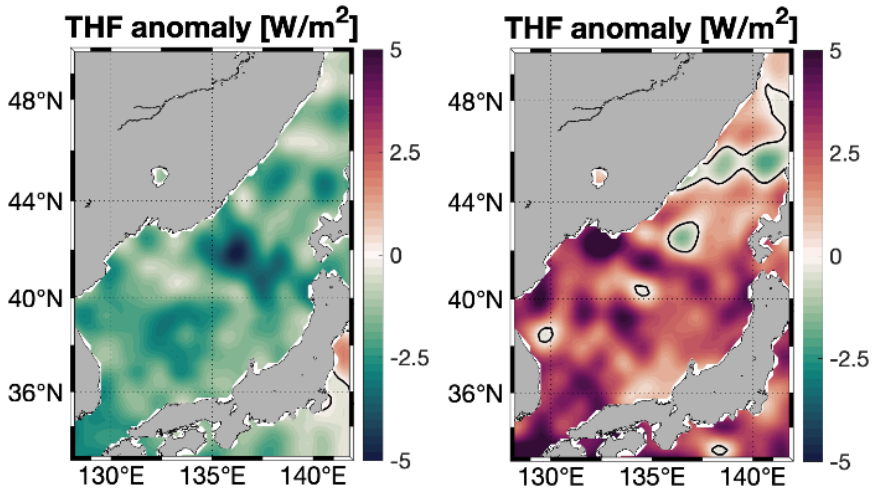

Figure 4.3. Regressed anomalies of the turbulent heat flux targeting the mode 1 (left) and the mode 2 (right).

The anomalies observed in the turbulent heat flux when composing mode 1 and mode 2 seem inconsistent with the regression patterns (Figure 4.4). This might suggest that the turbulent heat flux and the modes of variability may be influenced by additional or complex factors not captured in the current regression analysis.

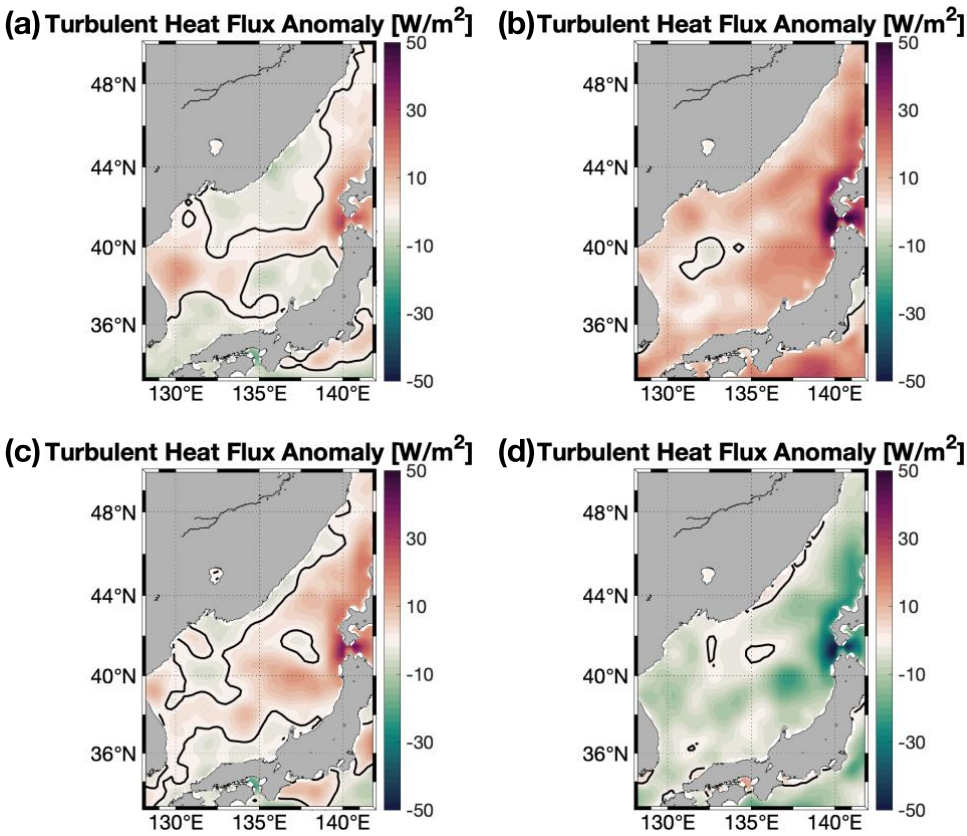

Figure 4.4. Composites of the turbulent heat flux anomalies. (a) positive composite based on the mode 1, (b) negative composite based on the mode 1, (c) positive composite based on the mode 2, and (d) negative composite based on the mode 2.

Figure 4.5 illustrates the correlation between the time series of each mode and climate indices, Arctic Oscillation (AO), Pacific Decadal Oscillation (PDO), and El Niño 3.4. The first mode exhibits a negative correlation with the AO, while the second mode shows a negative correlation with the PDO. This results need to be further examined for its physical interpretation.

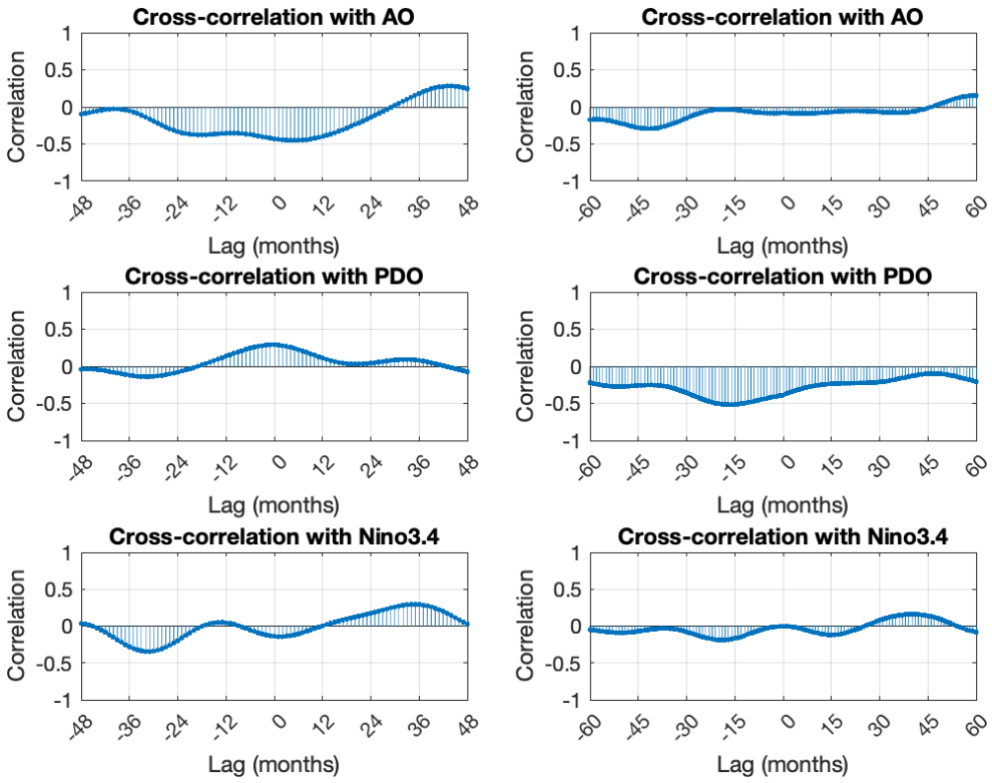

Figure 4.5. Lag correlation of the EOF mode 1 (left) and mode 2 (right) with the climate indices. The positive lag denotes each mode leads the climate indices.

Based on the results presented, the following conclusions were drawn. First, the variability of the KSBCW was investigated from 1982 to 2021 using EOF analysis. The first EOF mode represents the interannual variability of the KSBCW, and the second EOF mode displays the intensification of both the KSBCW and Tsushima Warm Water. Second, during the 40-year period, a significant correlation was observed between the variability of the KSBCW and the upper-ocean temperature variation in the southwestern part of the East Sea.

Lastly, interannual and long-term variability of the KSBCW over the 40 years were significantly correlated with the variability in basin-scale wind fields.

The intricate relationship between the turbulent heat flux and the variations in the KSBCW and the connection between various climate indices and KSBCW fluctuations are areas of study that necessitate further exploration. Although intuitively present based on fundamental links between atmospheric, oceanic, and climatic systems, these relationship needs to be substantiated with comprehensive analysis and data-driven evidence.

Bibliography

Chang, K. I., Teague, W. J., Lyu, S. J., Perkins, H. T., Lee, D. K., Watts, D. R., Kim, Y. B., Mitchell, D. A., Lee, C. M., & Kim, K. (2004). Circulation and currents in the southwestern East/Japan Sea: Overview and review. *Progress in oceanography* 61(2-4):105-156.

Chen, S., Wang, H., Chen, W., Zhang, Y., & Zhang, Y. (2022). Decadal intensified and slantwise Subpolar Front in the Japan/East Sea. *Frontiers in Marine Science* 9.

Cho, Y.-K., & Kim, K. (1998). Structure of the Korea Strait Bottom Cold Water and its seasonal variation in 1991. *Continental Shelf Research*, *18*(7):791-804.

Cho, Y.-K., & Kim, K. (2000). Branching Mechanism of the Tsushima Current in the Korea Strait. *Journal of physical oceanography* 30(11):2788-2797

Gordon, A. L., & Giulivi, C. F. (2004). Pacific decadal oscillation and sea level in the Japan/East sea. *Deep Sea Research Part I: Oceanographic Research Papers* 51(5):653-663.

He, S., Gao, Y., Li, F., Wang, H., & He, Y. (2017). Impact of Arctic Oscillation on the East Asian climate: A review. *Earth-Science Reviews* 164:48-62.

Isobe, A. (1994). Seasonal variability of the barotropic and baroclinic motion in the Tsushima-Korea Strait. *Journal of Oceanography* 50:223-238.

Isobe, A. (1995). The influence of the bottom cold water on the seasonal variability of the Tsushima Warm Current. *Continental Shelf Research* 15(7):763-777.

Johnson, D. R., & Teague, W. J. (2002). Observations of the Korea Strait bottom cold water. *Continental Shelf Research* 22(5):821-831.

Kim, C. H., & Kim, K. (1983). CHARACTERISTICS AND ORIGIN OF THE COLD WATER MASS ALONG THE EAST COAST OF KOREA. *The Journal of the Oceanological Society of Korea* 18:73-83.

Kim, I.-N., & Lee, T. (2004). Physicochemical Properties and the Origin of Summer Bottom Cold Waters in the Korea Strait. *Ocean and polar research* 26(4):595-606.

Kim, Y.-G., & Kim, K. (1999). Intermediate Waters in the East/Japan Sea. *Journal of Oceanography* 55:123-132.

Kim, Y.-Y., Cho, Y.-K., & Kim, Y. H. (2018). Role of cold water and beta-effect in the formation of the East Korea Warm Current in the East/Japan Sea: a numerical experiment. *Ocean Dynamics* 68:1013-1023.

Kim, Y. H., Kim, Y.-B., Kim, K., Chang, K.-I., Lyu, S. J., Cho, Y.-K., & Teague, W. J. (2006). Seasonal variation of the Korea Strait Bottom Cold Water and its relation to the bottom current. *Geophys. Res. Lett* 33(24).

Lee, J.-S., Suh, Y.-S., Go, W.-J., Hwang, J.-D., Youn, S.-H., Han, I.-S., Yang, J.-Y., Song, J.-Y., Park, N.-H., & Lee, K.-J. (2010). Improvement Plan

of NFRDI Serial Oceanographic Observation (NSO) System for Operational Oceanographic System. *Journal of the Korean Society of Marine Environment & Safety* 16:248-258.

Lim, D. B., & Chang, S.-d. (1969). ON THE COLD WATER MASS IN THE KOREA STRIT. *The Journal of the Oceanological Society of Korea* 4:71-82.

Lyu, S. J., & Kim, K. (2002). Atmospheric pressure-forced subinertial variations in the transport through the Korea Strait. *Geophysical Research Letters* 29.

Min, H.-S., Kim, Y.-H., & Kim, C.-H. (2006). Year-to- Year Variation of Cold Waters around the Korea Strait. *Ocean science journal* 41(4):227-234.

Min, H.-S., Park, J.-H., Choi, A. R., Park, Y.-G., Shin, K.-S., & Jang, P.-G. (2011). Observation of Water Property Variations in the Western Channel of the Korea Strait During 2006-2010. *Ocean and polar research* 33:325-336.

Na, H., Isoda, Y., Kim, K., Kim, Y. H., & Lyu, S. J. (2009). Recent observations in the straits of the East/Japan Sea: A review of hydrography, currents and volume transports. *Journal of marine systems* 78(2):200-205.

Na, H., Kim, K.-Y., Chang, K.-I., Kim, K., Yun, J.-Y., & Minobe, S. (2010). Interannual variability of the Korea Strait Bottom Cold Water and its relationship with the upper water temperatures and atmospheric forcing in the Sea of Japan (East Sea). *Journal of Geophysical Research* 115(C9).

Na, H., Kim, K.-Y., Minobe, S., & Sasaki, Y. N. (2018). Interannual to Decadal Variability of the Upper-Ocean Heat Content in the Western North Pacific and Its Relationship to Oceanic and Atmospheric Variability. *Journal of climate* 31:5107-5125.

Nam, S., Yoon, S. T., Park, J. H., Kim, Y. H., & Chang, K. I. (2016). Distinct characteristics of the intermediate water observed off the east coast of Korea during two contrasting years. *Journal of Geophysical Research: Oceans* 121(7):5050-5068.

Pak, G., Park, Y.-H., Vivier, F., Kwon, Y.-O., & Chang, K.-I. (2014). Regime-Dependent Nonstationary Relationship between the East Asian Winter Monsoon and North Pacific Oscillation. *Journal of climate* 27(21): 8185-8204

Park, J.-H. (2018). Dynamics of seasonal and interannual variations of currents observed near the east coast of Korea.

Park, J.-H., Kim, Y. S., Lee, H. J., Lee, H.-Y., & Ha, H. K. (2016). Internal Tide-Induced Enhancement of Cold Water Intrusion on the Continental Shelf of the Korea Strait. *Journal of Coastal Research*(Special Issue, No. 75):542-546.

Park, J.-H., Kim, Ye Sol, Lee, Ho Jin, Lee, Hee-Yeol, Ha, Ho Kyung, et al. (2016). Internal Tide-Induced Enhancement of Cold Water Intrusion on the Continental Shelf of the Korea Strait. *Journal of Coastal Research* 75:542-546.

Park, K.-A., Park, J.-E., & Kang, C.-K. (2022). Satellite-Observed

Chlorophyll-a Concentration Variability in the East Sea (Japan Sea): Seasonal Cycle, Long-Term Trend, and Response to Climate Index. *Frontiers in Marine Science*. 9.

Park, Y.-G., Cho, Y.-K., & Kim, K. (1995). A hydraulic model of the Korea Strait bottom cold current. *Journal of Oceanography*, *51*(6), 713-727.

Perkins, H., Teague, W. J., Jacobs, G. A., Chang, K. I., & Suk, M. S. (2000). Currents in Korea-Tsushima Strait during summer 1999. *Geophys. Res. Lett.* 27(19):3033-3036.

Teague, W. J., Ko, D. S., Jacobs, G. A., Perkins, H. T., Book, J. W., Smith, S. R., Chang, K.-I., Suk, M.-s., Kim, K., Lyu, S. J., & Tang, T. Y. (2006). Currents Through the Korea/Tsushima Strait: A Review of LINKS Observations. *Oceanography* 19:50-63.

Yeo, S.-R., Kim, W., & Kim, K.-Y. (2017). Eurasian snow cover variabiility in relation to warming trend and Arctic Oscillation. *Climate Dynamics* 48:499-511.

Yoon, J.-H., Abe, K., Ogata, T., & Wakamatsu, Y. (2005). The effects of wind-stress curl on the Japan/East Sea circulation. *Deep-Sea research. Part II* 52:1827-1844.

Yoon, J.-H., & Kim, Y.-J. (2009). Review on the seasonal variation of the surface circulation in the Japan/East Sea. *Journal of marine systems* 78:226-236.

Yoon, S.-T., Chang, K.-I., Na, H., & Minobe, S. (2016). An east-west contrast of upper ocean heat content variation south of the subpolar front in the East/Japan Sea. *Journal of Geophysical Research: Oceans* 121(8): 6418-6443.

Yun, J.-Y., Magaard, L., Kim, K., Shin, C.-W., Kim, C., & Byun, S.-K. (2004). Spatial and temporal variability of the North Korean Cold Water leading to the near-bottom cold water intrusion in Korea Strait. *Progress in oceanography* 60(1):99-131.

Abstract

대한해협은 쿠로시오 해류의 지류인 쓰시마 난류가 동해로 유입되는 통로이다. 대한해협의 주요 수괴로는 쓰시마 난류가 수송하는 쓰시마 온난수(수온 10℃ 이상, 염분 34.3 psu 이상)와, 주로 서수도 깊은 수심에서 발견되는 수온 10℃ 이하의 대한해협 저층냉수가 있다. 이 연구에서는 1982년부터 2021년까지의 기간 동안 한국해양자료센터에서 제공하는 정선해양관측 수온 자료를 사용하여 대한해협 저층냉수의 장기 변동을 분석하고, 동해 남서쪽 울릉분지 상층 수온 변동과의 관계를 살펴보았다. 또한 ERA5 바람 자료를 사용하여 분지규모 바람장과의 상관관계를 분석하였다. 208 정선 대한해협 수온 수직 단면 분석 결과 계절 변동보다 긴 주기에서 가장 주요한 모드가 대한해협 저층냉수의 경년 변동인 것으로 나타났다. 이 모드에 회귀분석한 바람은 분지 규모에서 반시계 방향의 회전 성분을 보였다. 두번째로 주요한 모드는 1990년대 이후 대한해협 저층냉수와 쓰시마 온난수가 모두 강화되는 수직 성층이 강화를 나타냈다. 이 모드에 회귀분석한 바람은 분지 규모에서 시계 방향의 회전 성분을 보였다. 이러한 분지 규모 바람장과의 상관성을 바탕으로, 앞으로의 연구에서는 대한해협 저층냉수의 장기 변동이 북태평양 기후 변동과 어떠한 상관성을 가지는지에 대한 분석이 필요할 것으로 생각된다.